Res Chem Intermed (2013) 39:1711–1726
DOI 10.1007/s11164-012-0904-3

Photocatalytic degradation intrinsic kinetics of gaseous cyclohexane in a fluidized bed photocatalytic reactor

Qijin Geng · Qingming Wang · Yunchen Zhang · Lintong Wang · Huiqin Wang

Received: 21 June 2012 / Accepted: 5 August 2012 / Published online: 16 November 2012

Abstract The special photocatalytic degradation intrinsic kinetics of gaseous cyclohexane were investigated in a designed fluidized bed photocatalytic reactor (FBPR). A series of photocatalytic kinetic reaction equations were developed to explore the relationship of degradation efficiency and operating variables based on photocatalytic mechanism and particle fluidization hydrodynamic characteristics. The corresponding results indicated that the initial concentration has influenced the photocatalytic degradation reaction conversion, and having a concentration inflexion point which theoretically divided the photocatalysis into a first-order apparent kinetic rate equation at low concentrations and a zero-order kinetic rate equation at high concentrations. Furthermore, these results were validated theoretically by the intrinsic kinetic models of photocatalytic degradation conversion developed according to variation of cyclohexane concentration and gas velocity. Based on the experimental results, the optimal operating gas velocity range was determined. The multi-factors synergy effect resulting from gas velocity on photocatalytic degradation efficiency was explored and proved by mass transfer, illumination transmission and adsorption models. Finally, the degradation pathways of the cyclohexane and deactivation mechanism of the photocatalyst were studied

Q. Geng (✉) · Q. Wang · Y. Zhang · L. Wang · H. Wang
Department of Chemistry-Chemical & Environmental Engineering, Weifang University, Weifang 261061, People's Republic of China
e-mail: jngengqijin@yahoo.com

Q. Wang
e-mail: wangqm@wfu.edu.cn

Y. Zhang
e-mail: wanglt@163.com

L. Wang
e-mail: yunchzhang@wfu.edu.cn

H. Wang
e-mail: wanghq@wfu.edu.cn

according to the intermediates degraded on TiO_2 surface, and a feasible method presented for catalyst regeneration.

Keywords Photocatalytic degradation · Cyclohexane · FBPR · Titania · Kinetics model

List of symbols

A_i	Peak area of component i (%)
C_e	Equilibrium concentration (ppmv)
C_0	Initial concentration of component i (ppmv)
C_t	Remaining concentration at t min (ppmv)
K_i	Adsorption equilibrium constant of the component i (ppmv min^{-1})
D_{eff}	Diffusion coefficient (m^2 s^{-1})
k_i	Reaction rate constants of component i (ppmv min^{-1})
$[h^+]$	Concentration of hole (mol L^{-1})
$[H_2O]$	Water concentration (ppmv)
I	Light intension (μmol m^{-2} s^{-1})
$[\cdot OH]$	Concentration of hydroxyl radical (mol L^{-1})
r	Photocatalytic degradation reaction rate (ppmv min^{-1})
R	Bed diameter (mm)
RH	Related humidity (%)
R_{out}	Outer diameter of reactor (mm)
U_g	Gas velocity (mm s^{-1})
U_{mf}	Minimum fluidization velocity (mm s^{-1})
t	Time (min)
T	Ratio of transimission (%)
z	Bed height (cm)
θ_i	Surface coverage (%)
ε	Averaged bed voidage (%)
ρ	Density (kg m^{-3})
ŋ	Degradation efficiency of component i (%)
λ	Thickness of reactor inner-sleeve

Introduction

Photocatalytic decomposition of trace contaminants from polluted air has been investigated extensively in the last three decades [1–8]. The attractive advantage of photocatalytic oxidation is a complete and efficient remediation technology of a broad range of pollutants at ambient temperature and pressure without any chemical additives. In addition, a TiO_2 photocatalyst, which is commonly employed, is inexpensive, safe, and very stable with high photocatalytic activity. Therefore, these photocatalytic degradation systems are actively used as an economical remediation method for various purification applications.

As compared to the fixed bed photoreactors, the fluidized bed photoreactors can offer superior mass transfer efficiency and light transmission, which was originally proposed and theoretically evaluated by Yue and Khan [9], and demonstrated by Dibble and Raupp [3] using a bench-scale flat plate fluidized bed photoreactor for photocatalytic oxidation of trichloroethylene (TCE). Further, Lim et al. [4] have developed a modified two-dimensional fluidized bed photocatalytic reactor (FBPR) system and determined the effects of various operating variables on the decomposition of NO. The photocatalytic degradation of TCE in a fluidized bed reactor was also investigated by Lim and Kim [5, 6], respectively. Nelson et al. [7] have investigated the photocatalytic oxidation of methanol using titania-based fluidized beds. In addition, the fluidized bed configuration can enable a most efficient use of the light source in photochemical reactions. Zhang et al. [8] have systematically investigated photocatalytic degradation of mixed gaseous carbonyl compounds at low level on an adsorptive TiO_2/SiO_2 photocatalyst using an annular fluidized bed reactor. Imoberdorf [10, 11], Pareek [12], and Pasquali [13] et al. have further studied the relationship between radiation fields and reaction kinetics in fluidized bed photoreactors and have proposed the mathematical models. As a result, the photocatalytic oxidation of airborne contaminants in fluidized bed photoreactors appears to be a promising process for the remediation of volatile pollutants in an indoor environment.

In the gas–solid heterogeneous photocatalysis, the mass transfer resistance from the gas bulk phase to the solid photocatalyst surface influences the photocatalytic oxidation reaction rate or conversion. The mass transfer resistance will vary with increasing gas velocity, thus the gas velocity, as an important factor for a fluidized bed reactor, should be investigated in terms of the relationship between particle fluidization hydrodynamic characteristics and illumination transmission. But there is little literature reporting the synergy effect resulting from gas velocity in photocatalysis.

Moreover, it should be noted that the C–H bond activation leading to photocatalytic oxidation of cyclohexane was one of the most challenging chemical problems. Up to now, some results have been reported in the area of oxidation of alkanes under mild conditions [14, 15]. Sannino et al. [16] reported on the sulphated MoO_x/TiO_2 catalysts in the selective oxidation of cyclohexane to benzene in a fixed bed reactor, and in a two-dimensional fluidized bed photoreactor. Brusa and Grela [17] investigated the photon flux and wavelength effects on the special selectivity and product yield in photocatalytic oxidation of cyclohexane on TiO_2 particles. Li et al. [18] published the corresponding results concerning the photocatalytic oxidation of cyclohexane over TiO_2 nano-scale particles by molecular oxygen. Selishchev et al. [19] explored the influence of adsorption on the photocatalytic properties of TiO_2/AC composite materials in cyclohexane vapor photooxidation reactions. In addition, Carneiro et al. [20] explored the effect of Au on TiO_2 catalyzed selective photocatalytic oxidation of cyclohexane.

However, there is little information in the open literature concerning the influencing factors of the photocatalytic oxidation of gaseous cyclohexane in a FBPR. So far, the intrinsic kinetic models of the operating variables in photocatalysis have been not reported in the published literature.

In the present work, we focus on an investigation of the photocatalytic degradation of gaseous cyclohexane which is widely used as a solvent for paints, resins, rubbers, plastics, and pharmaceuticals. The photocatalytic degradation intrinsic kinetics model of gaseous cyclohexane in FBPR and the corresponding operating variables were considered. The multi-factors synergy effect of gas velocity in this FBPR wasn explored based on particle fluidization hydrodynamic characteristics, equilibrium adsorption and illumination transmission. Subsequently, an optimal operating range of gas velocity was obtained. Furthermore, based on the degraded products detected, the photocatalytic degradation mechanism of cyclohexane and the causes of catalyst deactivation were deduced.

Experimental

FBPR design

In the present work, the schematic diagram of FBPR presented in Fig. 1 is a concentric double-pipe structure reactor, equipped with an ultraviolet lamp (25 W and with a maximum emission intensity at the wavelength of 254 nm; Shanghai Yaming Lighting, China) at the center of the inner and outer sleeves of the annular fluidized bed reactor. The distance between the lamp surface and the inner sleeve (Pyrex glass tubes with a thickness of 4 mm) is 100 mm. The annular distance, volume, and length of the annular photocatalytic fluidized bed reactor were 20 mm, 3,800 mL, and 640 mm, respectively. Nano-sized TiO_2 (Degussa P-25, Shanghai, China), as a photocatalyst mixed with bulk titanium dioxide, was fed into the annular reaction region between the exterior sleeves of the Pyrex glass tubes and the inner sleeve of the reactor. The related properties of this photocatalyst and doped bulk titanium dioxide are listed in Table 1. Air mixed with cylcohexane was used as a gaseous fluidized medium. The experimental unit permits the generation of polluted air with a specific cyclohexane concentration and humidity content.

Analytical methods

Several operating variables in this photocatalysis have been tested. Gas velocity (U_g) is controlled by a rotor flow meter. RH is determined using a temperature and humidity detector (Type 608-H1; Shanghai, China). Pressure drop is measured by a pressure transducer with an A/D converter and multi-function data processor (Type LD 185B; Shanghai, China). The averaged bed voidage was calculated according to the following equations.

$$\overline{\varepsilon} = 1 - (1 - \frac{\rho_B}{\rho_R})\frac{x}{5} \quad (1)$$

where $\overline{\varepsilon}$ is the averaged bed voidage; x is the value of sensor signal yielded by particulate velocity detector (PV-6A; Institute of Process Engineering, Chinese Academy of Science, China); ρ_B/ρ_R is the ratio between bulk density and real density of nano-scale titania and bulk titanium dioxide particles presented in Table 1.

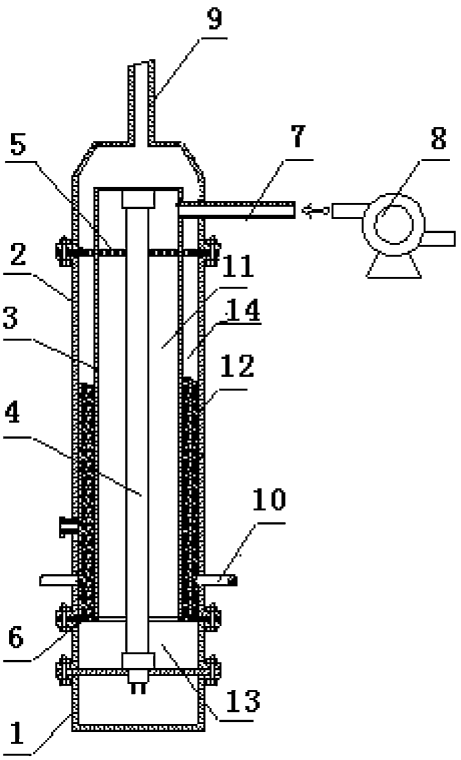

Fig. 1 Schematic diagram of FBPR

Table 1 Properties of titania (P25) and bulk titanium dioxide (BTD)

Fluidized material	Initial diameter D (nm)	Real density ρ_R (kg m^{-3})	Bulk density ρ_B (kg m^{-3})	Minimum fluidization velocity U_{mf} (mm s^{-1})
P25	20–30	3,800	1,250	36.2
BTD	38,000	3,800	1,650	41.8

A gas chromatograph equipped with a flame ionization detector (GC-FID, Clarus-500; PerkinElmer, USA) was used to determine cyclohexane concentration during the photocatalytic oxidation process. The GC operational parameters were as follows. The analytical column was a capillary column with length × ID × OD of 30 m × 0.32 mm × 0.4 μm and column temperature at 150 °C. The carrier gas and flame gas were hydrogen. The injected volume was 10 μL. FID detector temperature was 300 °C supplied with air/hydrogen.

At the regular time intervals of 15 min, 10 μL of cyclohexane was sampled to measure the corresponding peak area by GC-FID. The peak area (A_t) of the GC-FID is proportional to the concentration of cyclohexane. Subsequently, the cyclohexane

degradation efficiency (ŋ) in FBPR was calculated according to the following equation:

$$\eta = \frac{C_0 - C_t}{C_0} \times 100\% = \left(1 - \frac{A_0}{A_t}\right) \times 100\% \quad (2)$$

The by-products and intermediates generated during the photocatalytic degradation of cyclohexane were identified using ultraviolet–visible spectrophotometer (TU-1901; Beijing Purkinje General Instrument, China).

Results and discussion

Photocatalytic degradation kinetics

The traditional simplified mechanism of heterogeneous photocatalysis typically involves the photoexcitation of the conductor catalyst, which leads to averaged bed voidge formation of free charge carriers (electrons, e^-, and holes, h^+). Based on the mentioned mechanism and without considering the intermediates and products adsorption, the following elementary reactions presented in Table 2 have been taken into account: *R*1 refers to the photonic activation step; *R*2 depicts the recombination step between e^- and h^+; *R*3 represents the formation of hydroxyl radicals; *R*4 characterizes the transformation of the organic compound (Org) into product (P) by OH· attack; and in *R*5 the recombination between two hydroxyl radicals is suggested [21].

The photocatalytic degradation rate (r) of the organic compound is represented by the following expression according to step *R*4.

$$r = k_4[\cdot OH][\theta]_M \quad (3)$$

where the target compound adsorption coverage, $[\theta]_M$ can be given using averaged bed voidge Langmuir–Hinshelwood (L–H) model without considering a competition adsorption between water and the target molecules at low concentrations and low humidity

$$[\theta]_M = \frac{K_A[C]}{1 + K_A[C]} \quad (4)$$

Table 2 Mechanism of photocatalytic oxidation

Step	Elementary reaction
R1	$TiO_2 + h\nu \xrightarrow{k_1} e^- + h^+$
R2	$e^- + h^+ \xrightarrow{k_2}$ heat
R3	$h^+ + H_2O \xrightarrow{k_3} \cdot OH + H^+$
R4	$\cdot OH + Org \xrightarrow{k_4} P$
R5	$\cdot OH + \cdot OH \xrightarrow{k_5} H_2O_2$

$$[\theta]_{H_2O} = \frac{K_H[H_2O]}{1+K_H[H_2O]} \tag{5}$$

In contrast, based on averaged bed voidge binary-molecule L–H model, the target compound adsorption coverage can be given by Eqs. 6 and 7 with consideration of the competition adsorption between water and the target molecules.

$$[\theta]_M = \frac{K_A[C]}{1 + K_H[H_2O] + K_A[C]} \tag{6}$$

$$[\theta]_{H_2O} = \frac{K_H[H_2O]}{1+K_A[C]+K_H[H_2O]} \tag{7}$$

The concentration of photo-induced holes, $[h^+]$, can be obtained based on the mentioned elementary reactions *R*1–3 and the steady state assumption.

$$\frac{d[h^+]}{dt} = k_1 I[C_{TiO_2}] - k_2[h^+]^2 - k_3[h^+][H_2O] \cong 0 \tag{8}$$

Under high irradiation intensities, the recombination of the electron–hole is predominant, that is, $k_2[h^+]^2 \gg k_3[h^+][H_2O]$. As a result, the concentration of holes can be given by

$$[h^+] = \left(\frac{k_1 I[C_{TiO_2}]}{k_2}\right)^{\frac{1}{2}} \tag{9}$$

Considering the formation, oxidation and the recombination of hydroxyl radicals based on the elementary reactions *R*3–5, the concentration of ·OH can be obtained according to the steady state assumption.

$$\frac{d[\cdot OH]}{dt} = k_3[h^+][H_2O] - k_4[\cdot OH][C] - k_5[\cdot OH]^2 \cong 0 \tag{10}$$

where the recombination of hydroxyl radicals and oxidation of the target compound are competitive. The excessive OH· radical generation at high intensity led to their self-recombination [21]. At low concentration of target compound, the recombination of hydroxyl radicals can be assumed as the predominant reaction ($k_4[\cdot OH][C] \ll k_5[\cdot OH]^2$). Subsequently, the concentration of holes can be obtained as follows

$$[\cdot OH] = \left(\frac{k_3[h^+][\theta]_{H_2O}}{k_5}\right)^{\frac{1}{2}} \tag{11}$$

Influence of cyclohexane concentration

The influence of initial concentration on the photocatalytic degradation efficiency was investigated ranging from 2 to 300 ppmv. The experimental results presented in Fig. 2 indicated that the photocatalytic degradation efficiency in FBPR decreases with increasing initial concentrations of cyclohexane at the given gas velocity.

Theoretically, at low concentrations, the reaction rate equation can be given by following expression according to Eqs. 3, 4, 5, 9, and 11.

$$r=k_4\left[\frac{k_3\left(\frac{k_1 I[C_{TiO_2}]}{k_2}\right)^{\frac{1}{2}}}{k_5}\right]^{\frac{1}{2}}\frac{K_H^{\frac{1}{2}}[H_2O]^{\frac{1}{2}}K_A[C]}{(1+K_A[C])(1+K_H[H_2O]^{\frac{1}{2}}} \quad (12)$$

From Eq. 12, the reaction rate, dependent on cyclohexane concentration, is an apparent first-order kinetic expression at a given condition. This can be attributed to the fact that the colliding probability between hydroxyl radicals and cyclohexane molecules increases with increasing cyclohexane concentration. This behavior is in agreement with the results proposed by Kim and Hong [22].

The corresponding integral equation can be yielded and modified as a function of photocatalytic oxidation conversion over concentration variable based on Eq. 12.

$$\frac{1}{K_A}\ln\left(\frac{1}{1-\eta}\right)+C_0\eta=k_4\left[\frac{k_3\left(\frac{k_1 I[C_{TiO_2}]}{k_2}\right)^{\frac{1}{2}}}{k_5}\frac{K_H[H_2O]}{K_H[H_2O]+1}\right]^{\frac{1}{2}}t \quad (13)$$

According to Eq. 13, the photocatalytic oxidation conversion is dependent of the cyclohexane concentration. In this case, the photocatalytic oxidation conversion is controlled by the equilibrium distribution of cyclohexane between the gas and solid phases at a given reaction time.

At the given experimental conditions, i.e. illumination, humidity, amount of catalyst, and gas velocity, a plot of $^{t}/_{C_0\eta}$ versus $\ln\left(\frac{1}{1-\eta}\right)/_{C_0\eta}$ is linearly presented in Fig. 3 and will allow

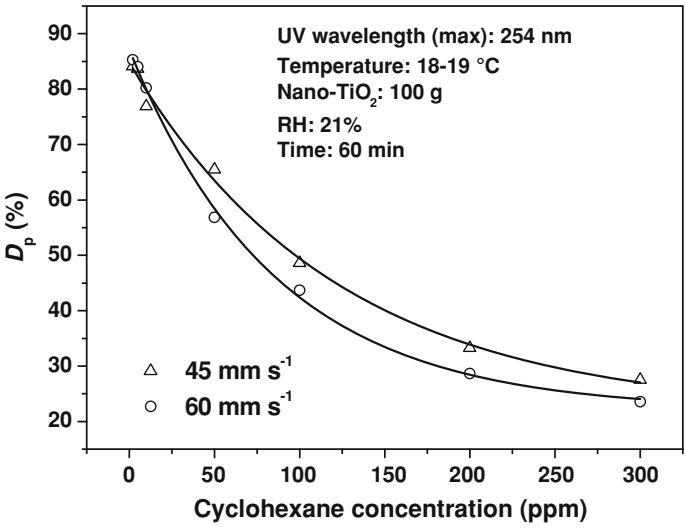

Fig. 2 Influence of cyclohexane concentration on photocatalytic degradation efficiency

$$k_4\left[\frac{k_3\left(\frac{k_1 I[C_{TiO_2}]}{k_2}\right)^{\frac{1}{2}}}{k_5}\right]^{\frac{1}{2}}\frac{K_H^{\frac{1}{2}}[H_2O]^{\frac{1}{2}}}{1+K_H[H_2O]^{\frac{1}{2}}}$$

and K_A to be determined as constants. The averaged values of them obtained are 1.085 ppmv min^{-1} and 2.985 $\times$ 10^{-2} $ppmv^{-1}$, respectively.

At high concentrations, if the adsorption of cyclohexane can be assumed as large as $K_A[C] \gg 1$, then Eq. 12 can be modified as follows.

$$r = k_4\left[\frac{k_3\left(\frac{k_1 I[C_{TiO_2}]}{k_2}\right)^{\frac{1}{2}}}{k_5}\right]^{\frac{1}{2}}\frac{K_H^{\frac{1}{2}}[H_2O]^{\frac{1}{2}}}{1 + K_H[H_2O]^{\frac{1}{2}}} \tag{14}$$

In this case, the reaction rate is independent of the reactant concentration, expressed as a zero-order kinetic equation, and may be attributed to the fact that the limited and fixed amounts of active sites are presented for degradation of cyclohexane at high concentrations as observed for the decomposition of TCE by UV/TiO_2 at the saturated adsorption [6].

The relationship between photocatalytic degradation conversion and initial concentration of cyclohexane can be yielded according to the integral of Eq. 14.

$$\eta = k_4\left[\frac{k_3\left(\frac{k_1 I[C_{TiO_2}]}{k_2}\right)^{\frac{1}{2}}}{k_5}\frac{K_H[H_2O]}{1 + K_H[H_2O]}\right]^{\frac{1}{2}}\frac{t}{C_0} \tag{15}$$

From Eq. 15, the photocatalytic oxidation conversion is approximated to a function of a reciprocal of the initial concentration and decreased with increasing cyclohexane concentration. This is similar to the experimental results presented in

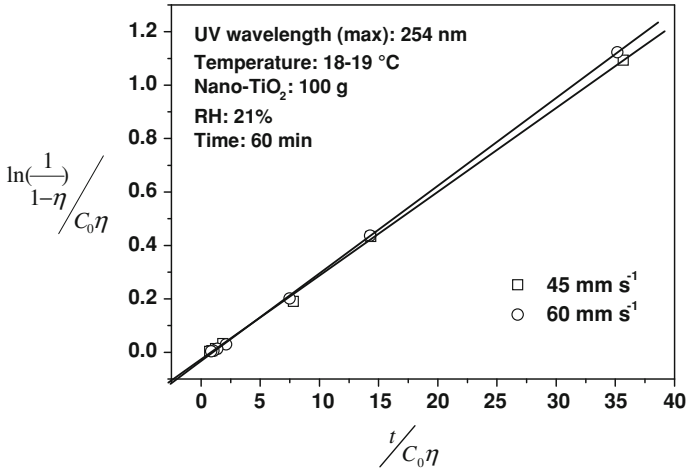

Fig. 3 Relationship of photocatalytic degradation efficiency and initial concentration of cyclohexane

Fig. 2, and may be attributed to the following reasons: (1) at high concentrations, the fixed surface adsorption active sites of catalyst are not sufficient for the amount of cyclohexane molecules, and part of the cyclohexane molecules flow out of the reaction region with bubbles at a given gas velocity; (2) the amount of products or intermediates formed in the photocatalysis increases with increasing initial concentration, and, as a result, they occupy part of the active sites of the catalyst to inhibit the oxidation progression; and (3) the cyclohexane molecules compete to adsorb with water molecules onto the surface active sites of the catalyst, which cause a retardation of the photocatalytic oxidation.

Uniting Eqs. 13 and 15, the concentration inflection point can be obtained under given conditions.

$$C_0 = k_4 \left[\frac{k_3 \left(\frac{k_1 I[C_{TiO_2}]}{k_2} \right)^{\frac{1}{2}}}{k_5} \right]^{\frac{1}{2}} \frac{K_H^{\frac{1}{2}}[H_2O]^{\frac{1}{2}}}{1+K_H[H_2O]^{\frac{1}{2}}} t \tag{16}$$

The value of the concentration inflexion point is calculated as 62.1 ppmv at the given reaction time of 60 min. Based on this inflexion point, the reaction order can be divided into a first-order reaction rate expression (Eq. 13) below it and a zero-order reaction rate equation (Eq. 15) above it.

Influence of gas velocity

For FBPR, the minimum fluidization velocity (U_{mf}) of the TiO_2 photocatalyst (P25) mixed with BTD at a mass ratio of 1/4 is 38.5 mm s^{-1}. With the variation of the gas velocity ranging from 3 to 80 mm s^{-1}, the photocatalytic degradation of cyclohexane was carried out, and the relationship of the photocatalytic degradation efficiencies and the gas velocity is shown in Fig. 4. From Fig. 4, it is found that the photocatalytic degradation efficiencies increased gently with increasing gas velocity ranging from 3 to 38.5 mm s^{-1} (U_{mf}). However, the photocatalytic degradation efficiencies increased dramatically with increasing the gas velocity ranging from 38.5 (U_{mf}) to 60 mm s^{-1} (1.56 U_{mf}). At high gas velocity, from 60 to 80 mm s^{-1} (2.08 U_{mf}), the photocatalytic degradation efficiencies slowly decrease. These experimental results indicate that the photocatalytic oxidation efficiencies of cyclohexane in FBPR exhibit the maximum values at a certain operating gas velocity range. This is interpreted that, at a certain gas velocity ranging from 36.2 (U_{mf}) to 60 mm s^{-1} (1.56 U_{mf}), the contact of the photocatalyst, UV light and reactants seemed to be at the optimal condition.

Firstly, for gas velocity ranging from 60 to 80 mm s^{-1}, a large amount of bubbles, formed in the fluidized bed reaction regions, may weaken the contact between the photocatalyst and the reactants since the target gas molecules can flow out of the reaction region with the bubbles. In addition, desorption was enhanced at high gas velocity. This can be proved by the variation of the adsorption curve in Fig. 4, where the adsorption efficiency decreases with increasing gas velocity ranging from 60 to 80 mm s^{-1}. Therefore, this process is obviously a mass transfer

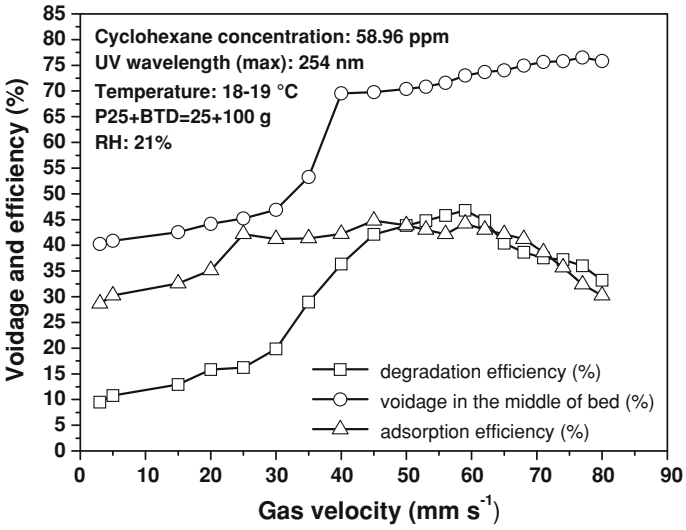

Fig. 4 Influence of gas velocity on degradation efficiency, adsorption efficiency, and averaged bed voidage

limited reaction due to desorption enhancement and the amount of bubbles increasing at high gas velocity.

Secondly, at gas velocity below the minimum fluidization velocity, the whole bed is approximated to a fixed bed and the gas molecules can break through the interspaces between the large particles out of the reaction region. However, the illumination transmission is inhibited at low bed voidage since UV-light cannot penetrate the reaction region deeply, as shown in Fig. 5. So this photocatalytic oxidation process is obviously limited by illumination resistance. In addition, from the adsorption curve in Fig. 4, we can also infer that mass transfer resistance exists when the gas velocity is below the minimum fluidization velocity in spite of the large resident time. This can be explained by it being difficult for cyclohexane molecules to diffuse into the interspaces of the photocatalyst agglomeration at low gas velocity. As a result, this photocatalytic degradation reaction with lower degradation efficiency is due to the illumination transmission and mass transfer resistances.

Thirdly, the gas velocity ranging from U_{mf} to 1.56 U_{mf} seemed to be an optimal condition for photocatalytic oxidation. In this case, the mechanisms of gas velocity on the photocatalytic degradation of cyclohexane in FBPR are very complex, since the bed expansion, axial distribution of bed voidage, radial distribution of incident light irradiation, residence time of reactants, and mass transfer between reactant and particulates are approximated to the maximum values at a certain gas velocity. There should be a multi-factors synergy effect among the catalyst particles fluidization hydrodynamic characteristics, equilibrium adsorption, and incident light irradiation transmission in FBPR. To explore this mechanism, the following bubbling model can be used to describe it in FBPR.

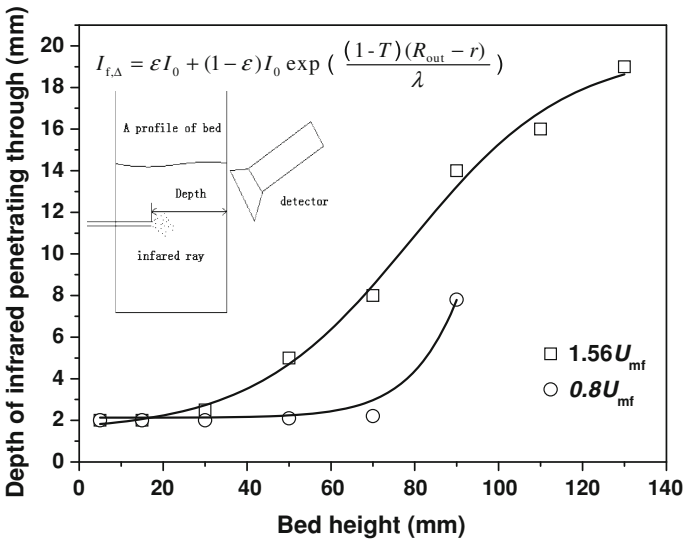

Fig. 5 Relationship of UV-light penetrating depth and bed height at various gas velocities

The photocatalytic oxidation occurred on the surface of the catalyst and the reactant molecules break through the bed with bubbles. Therefore, the mass transfer should be considered between the gas phase and the solid phase. The following equations are developed to describe the mass transfer among the bubble, cloud, and emulsion phases.

$$\begin{aligned} -\frac{1}{V_b}\frac{dN_{Ab}}{dt} &= -u_b\frac{dC_{Ab}}{dl} \\ &= (K_{bc})_b(C_{Ab}-C_{Ac}) \\ &= (K_{ce})_b(C_{Ac}-C_{Ae}) \\ &= (K_{be})_b(C_{Ab}-C_{Ae}) \end{aligned} \tag{17}$$

The corresponding boundary conditions are given by

$$\text{If } l=0 \text{ and } C_{Ab}=C_0\,, \text{ then } C_{Ab}=C_0\exp\left(-\frac{k_f l}{u_b}\right) \tag{17a}$$

$$\text{If } l=L_f \text{ and } C_{Ab}=C_{Ab,L}, \text{ then } C_{Ab,L}=C_0\exp\left(-\frac{k_f L_f}{u_b}\right) \tag{17b}$$

The reaction rate coefficient can be expressed as Eq. 18 at the given conditions.

$$k_f = k_r\left(\gamma_b + \frac{1}{\frac{k_r}{(K_{bc})_b} + \frac{1}{\gamma_c + \frac{1}{\frac{k_r}{(K_{ce})_b}+\frac{1}{\gamma_e}}}}\right) \tag{18}$$

The variation of cyclohexane concentration with illumination time in the photocatalytic oxidation process can be yielded considering the special influences of illumination transmission and gas velocity as follows.

$$C_t = C_0 \exp\left(-\frac{k_f I_{f,\Delta} L_f}{u_b}\right) \tag{19}$$

where $u_b = u_g - u_{mf} + 22.26 d_b^{\frac{1}{2}}$, and $I_{f,\Delta} = \varepsilon I_0 + (1-\varepsilon) I_0 \exp\left(1 - T(R_{out} - R)/\lambda\right)$

This model indicated that the multi-factors synergy mechanism in photocatalytic degradation of cyclohexane was involved in the variation of mass transfer, bed voidage, illumination transmission, resident time, and adsorption efficiency resulting from the gas velocity. This result is in agreement with the experimental values in Fig. 4. First, the adsorption efficiency is approximated to the maximum value at the gas velocity ranging from U_{mf} to 1.56 U_{mf}, which indicated that, for this gas–solid heterogeneous photocatalysis in FBPR, a large amount of the cyclohexane molecules adsorbed has a promotion role for the degradation reaction. Second, the illumination transmission is enough to guarantee the photocatalysis since the average bed voidage is approximated to the maximum values and varies gently with gas velocity, which can be confirmed by the penetrable depth presented in Fig. 5. As a result, at the given gas velocity ranging from U_{mf} to 1.56 U_{mf}, the high degradation efficiency may be attributed to the special synergy effect between high illumination transmission at the maximum bed voidage and the equilibrium adsorption value resulted from good mass transfer.

Photocatalytic degradation mechanism of cyclohexane

Since by-products could be a potential tool to explore the intrinsic kinetics of the photocatalytic oxidation, it is necessary to identify the intermediates yielded by the photocatalytic degradation of cyclohexane. Note that no gaseous intermediates have been detected by GC-FID in the gas phase, but without suggesting completed mineralization of the cyclohexane. The GC-FID apparatus used is not equipped with a CO_2 detector, so the detection and quantification of carbon dioxide cannot be highlighted during the photocatalytic degradation of cyclohexane. In the present experiment, by-products or intermediates were extracted from the catalyst surface using methanol solvent after the experiment. Then, the extracted solution was detected using an ultraviolet–visible spectrophotometer. As a result, we have identified cyclohexanol, cyclohexanone, and 2-cyclohexen-1-one as the main intermediate products in the catalyst surface based on the following information.

- 235 nm: the K absorption band of conjugation 2-cyclohexen-1-one;
- 278.6 nm: the R absorption band of cyclohexanone;
- 330 nm: the R absorption band of conjugation 2-cyclohexen-1-one;
- 250–275 and 300–500 nm: scatter and absorption effect by nano-particles;
- Cyclohexanol and methanol have no absorption band in the range from 200 to 500 nm.

Therefore, we can infer that the possible photocatalytic oxidation pathway of cyclohexane is as follows.

The photocatalytic degradation of alkane is initiated by the abstraction of protons to form alkyl radicals and water. The alkyl radicals can react with oxygen adsorbed on the catalyst surface to give alkal proxyl radicals which react with alkane or water to generate carboxylic acid. The reduction of an alkyl chain primarily takes place via decarboxylation according to the photo-Kolbe process.

In the present work, with the carbon atom of cyclohexane as secondary-carbon, a proposed mechanism for the photocatalytic oxidation of cyclohexane leads to the formation of cyclohexanol, which in turn oxidizes to cyclohexanone and 2-cyclohexen-1-one as presented in Fig. 6. The initial step is the abstraction of the protons to yield cyclohexanol. For the degradation process of cyclohexanol in photocatalysis, which is easier than that of cyclohexane in that the C–H bond strength (α-C) of cyclohexanol is weaker than that of cyclohexane. The produced radical can react with oxygen to yield hydroperoxyl radical. This radical can react with cyclohexanol or water to give cyclohexanone. The second step of further oxidation of cyclohexanone may be an abstraction of proton process, since the C–H bond activity (H–C–C=O) of cyclohexanone is higher than that of cyclohexane. Thereafter, 2-cyclohexen-1-one may be obtained.

Deactivation and regeneration of photo-catalyst

Slow decay of the activity was observed for all experimental conditions using a circulated oxidation reactant procedure. Possible causes of the observed activity decline were: (1) site blockage by by-products such as carbonaceous deposits; (2) consumption of active surface oxygen species at rates exceeding their replenishment; and (3) irreversible surface dehydroxylation [23].

In the present work, the deactivation of the catalyst was significant according to the degradation efficiency, presented with running two times in Fig. 7. In addition,

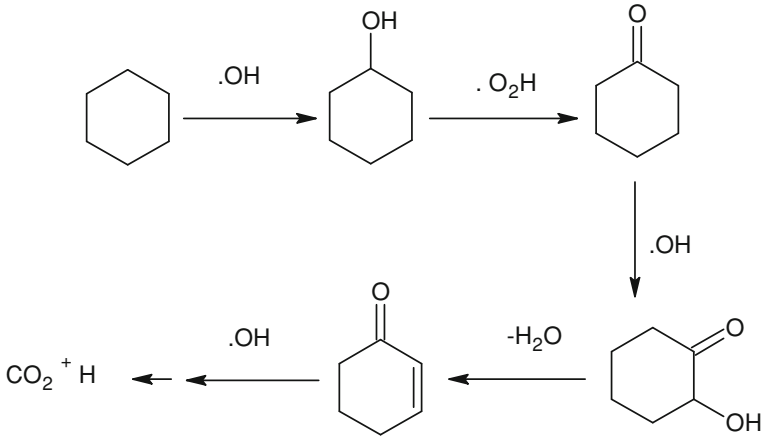

Fig. 6 Photocatalytic oxidation pathway of cyclohexane

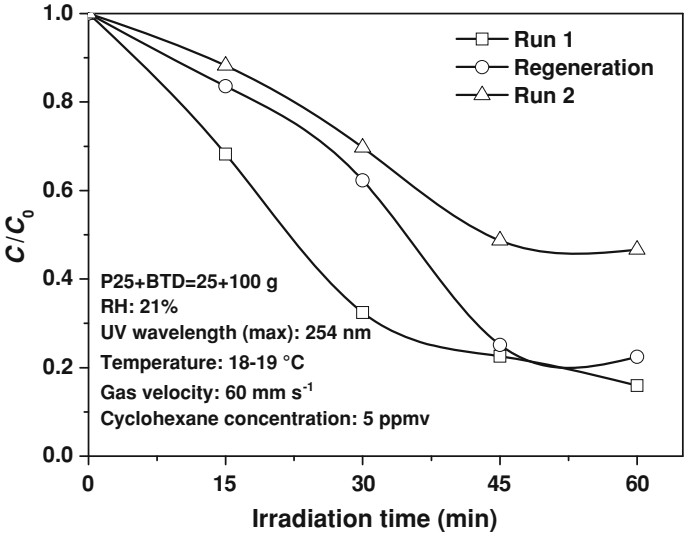

Fig. 7 Deactivation and regeneration of photocatalyst

the color of the photocatalyst surface was initially white, turning into yellow after 2 runs of photocatalytic oxidation. This deactivation of the photocatalyst in the process of the degradation of cyclohexane may be attributed to the following reasons. First, the degraded products, cyclohexanol, cyclohexanone, and 2-cyclohexen-1-one, adsorbed on the surface of the photo-catalyst, inhibit the cyclohexane molecular from adsorbing onto the reactive sites of the catalyst. The variation of catalyst color may be a good proof for adsorption of these organic molecules on the surface of the catalyst. It is similar to the result reported by Wang [24]. Second, these degraded products or intermediates, as a new kind of scavenger of holes or electrons, were detrimental to the photocatalytic oxidation of cyclohexane.

The regeneration was very important for the practical application of the photocatalyst. In this section, the regeneration of the particle photocatalyst was investigated. The photocatalyst used was simply treated at 473 K for 5 h in air, and it was found that the activity recovered to 80–90 % of the initial activity, as shown in Fig. 7. The feasibility of the regeneration method can be explained because the organic compounds adsorbed onto the surface active sites of the photocatalyst particles can be cleared away after treatment.

Conclusions

The photocatalytic degradation kinetics of gaseous cyclohexane using nano-titania agglomerates has been investigated in FBPR and the main conclusions can be derived from the present study. A series of photocatalytic kinetic reaction equations were developed to explore the relationship of the degradation efficiency and

operating variables based on the photocatalytic mechanism and particle fluidization hydrodynamic characteristics. The special optimal operating gas velocity ranging from U_{mf} to 1.56 U_{mf} was determined. The multi-factors synergy effect resulting from gas velocity on phtocatalytic degradation was explored and proved by the mass transfer, illumination transmission, and adsorption models.

Acknowledgments This investigation was supported by the Ph.D. Programs Foundation of Weifang University (Contract No. 2012BS07), Natural Science Foundation of Shandong Province (Contract No. ZR2011BM019), and Education Department Teacher Project of Shandong Province (Contract No. J11LB55).

References

1. M. Xing, Y. Wu, J. Zhang, F. Chen, Nanoscale **2**, 1233–1239 (2010)
2. Y. Wu, M. Xing, B. Tian, J. Zhang, Chem. Eng. J. **162**, 710–717 (2010)
3. L.A. Dibble, G.B. Raupp, Environ. Sci. Technol. **26**, 492–495 (1992)
4. T.H. Lim, S.M. Jeong, S.D. Kim, J. Gyenis, J. Photochem. Photobiol. **134**, 209–217 (2000)
5. T.H. Lim, S.D. Kim, Chem. Eng. Process. **44**, 327–334 (2005)
6. T.H. Lim, S.D. Kim, Chemosphere **54**, 305–312 (2004)
7. R.J. Nelson, C.L. Flakker, D.S. Muggli, Appl. Catal. **69**, 189–195 (2007)
8. M. Zhang, T. An, J. Fu, G. Sheng, X. Wang, X. Hu, X. Ding, Chemosphere **64**, 423–431 (2006)
9. P.L. Yue, F. Khan, Chem. Sci. Eng. **38**, 1893–1900 (1983)
10. G.E. Imoberdorf, F. Taghipour, M. Keshmiri, M. Mohseni, Chem. Eng. Sci. **63**, 4228–4238 (2008)
11. G.E. Imoberdorf, A.E. Cassano, O.M. Alfano, H.A. Irazoqui, AIChE J. **52**, 1814–1823 (2006)
12. V.K. Pareek, A.A. Adesina, AIChE J. **50**, 1273–1288 (2004)
13. M. Pasquali, F. Santarelli, J.F. Porter, P. Yue, AIChE J. **42**, 532–537 (1996)
14. L. Zhang, W.A. Anderson, S. Sawell, C. Moralejo, Chemosphere **68**, 546–553 (2007)
15. Q. Geng, Q. Guo, X. Yue, Ind. Eng. Chem. Res. **49**, 4644–4652 (2010)
16. D. Sanninoa, V. Vaiano, P. Ciambelli, P. Eloy, E.M. Gaigneaux, Appl. Catal. A **394**, 71–78 (2011)
17. M.A. Brusa, M.A. Grela, J. Phys. Chem. B **109**, 1914–1918 (2005)
18. X. Li, G. Chen, P.Y. Lock, C. Kutal, J. Chem. Technol. Biotechnol. **78**, 1246–1251 (2003)
19. D.S. Selishchev, P.A. Kolinko, D.V. Kozlov, J. Photochem. Photobiol. **229**, 11–19 (2012)
20. J.T. Carneiro, T.J. Savenije, J.A. Moulijn, G. Mul, J. Photochem. Photobiol. **217**, 326–332 (2011)
21. G. Vincent, P.M. Marquaire, O. Zahraa, J. Photochem. Photobiol. A **197**, 177–189 (2008)
22. S.B. Kim, S.C. Hong, Appl. Catal. B **35**, 305–315 (2002)
23. J. Peral, X. Domènech, D.F. Ollis, J. Chem. Technol. Biotechnol. **70**, 117–140 (1997)
24. W. Wang, L.W. Chiang, Y. Ku, J. Hazard. Mater. **101**, 133–146 (2003)